LANGMUIR
Article
Cite This: Langmuir 2019, 35, 16438−16443
pubs.acs.org/Langmuir

A Most Enantioselective Chiral Surface: Tartaric Acid on All Surfaces Vicinal to Cu(110)

Burcu Karagoz,[†] Matthew Payne,[†] Aaron Reinicker,[†] Petro Kondratyuk,[†] and Andrew J. Gellman*,[†,‡]

[†]Department of Chemical Engineering and [‡]W.E. Scott Institute for Energy Innovation, Carnegie Mellon University, 5000 Forbes Ave, Pittsburgh, Pennsylvania 15213, United States

Supporting Information

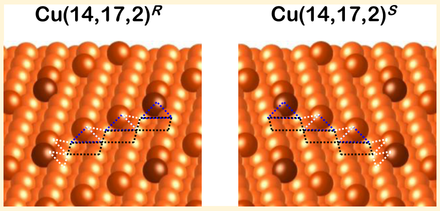

ABSTRACT: Enantioselective chemistry on intrinsically chiral surfaces is the quintessential form of structure-sensitive surface chemistry, arising purely from the dissymmetry of the surface structure. Identification or design of chiral surface structures that maximize enantioselectivity for a given processes is extremely challenging because of the limited magnitude of the enantiospecific interaction energetics of chiral molecules with chiral surfaces. Using spherical Cu single crystals exposing surfaces with a continuous two-dimensional distribution of crystallographic orientations, we mapped the enantiospecific surface reaction kinetics of tartaric acid decomposition across the surface orientation space. These measurements reveal both the mechanistic origin of enantioselectivity and identify the structural features of the most enantiospecific surface orientation.

INTRODUCTION

Understanding the relationship between atomistic surface structure and surface reaction kinetics is one of the longstanding goals of surface chemistry and catalysis. The demonstration that catalytic ammonia synthesis on Fe single-crystal surfaces is structure sensitive is one of the great early achievements in the field.[1,2] The grand challenge is to understand the relationship between surface structure and surface chemistry with the fidelity needed to predict the optimal catalytic material and its optimal surface structure for a given reaction. Herein, we tackle what is probably the most subtle form of structure sensitivity; enantioselective reactions of chiral compounds on chiral surfaces. Enantioselectivity is the quintessential form of surface structure sensitivity. It arises only from the difference in interactions between a chiral molecule and two enantiomorphous surface structures, i.e., non-superimposable mirror images of one another.

Chirality and enantioselectivity are of practical interest because of their critical importance for bioactive compounds such as pharmaceuticals, agrochemicals, fragrances, etc.[3,4] This arises because the biochemical makeup of life on Earth is based on a set of chiral compounds including DNA, amino acids, and sugars that appear in only one of their two enantiomeric forms. As a result, the two enantiomers of a chiral pharmaceutical can have vastly different physiological impact, necessitating their production and administration in an enantiomerically pure form.[3] Enantioselective synthesis and purification processes are key steps in pharmaceuticals production. They require the use of enantiomerically pure chiral materials to differentiate between the enantiomers of reactants, intermediates, and products of enantioselective reactions. Production steps requiring catalytic surface reactions can be rendered enantioselective using chiral surfaces.[5,6] The challenge in developing such processes is the design of chiral surfaces with structures tuned to optimize the enantioselectivity of the overall process. Herein, we demonstrate a means for identifying the enantiospecifically optimum structure of a chiral metal surface from among a continuum of crystallographic surface orientations.

Chiral surfaces are often prepared by modifying an achiral surface with an enantiomerically pure chiral compound.[5] The chirality of the adsorbed modifier imparts enantiospecificity to processes occurring on that surface. However, there are also many inorganic materials with chiral structures and chiral surfaces.[7−10] Even achiral materials such as metals can expose surfaces with structures that are intrinsically chiral, provided only that there are no bulk mirror planes oriented perpendicular to the surface (Figure 1a).[7,9] In the case of cubic metals, all crystallographic orientations with Miller indices $h \neq k \neq l \neq h$ and $h \times k \times l \neq 0$ yield intrinsically chiral surface structures.[7] These have ideal structures comprised of low Miller index terraces separated by monoatomic steps formed by the intersections of step and kink microfacets with different orientations. Such intrinsically chiral surfaces exhibit a variety of enantiospecific interactions with chiral adsorbates.[6,11−13]

Chiral metal surfaces have an infinite number of possible surface structures, spanning the two-dimensional (2D) continuum of the two angles defining the orientations of surface normal vectors within a bulk crystal lattice. In terms of the stereographic triangle representing all possible planes that can be cleaved through a lattice (sect SI 1), all points in the interior of the triangle represent chiral surfaces.[14] The ideal structures of these surfaces have six motifs; they have terraces

Received: August 8, 2019
Revised: October 1, 2019
Published: November 15, 2019

ACS Publications

DOI: 10.1021/acs.langmuir.9b02476

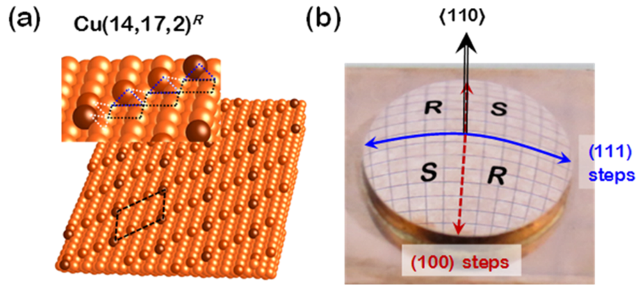

Figure 1. (a) Graphic illustration of the ideal structure of the chiral Cu(14,17,2)^R surface. The unit cell is outlined in black, and the microfacets forming the kink are outlined in color: (110) black, (100) blue, and (111) white. (b) Photograph of a Cu(110) ± 14°-S^{4}C (10 mm diameter × 2 mm thickness) with the reflection of a piece of graph paper. The achiral high-symmetry surfaces are the Cu(110) point at the center, the Cu(*hk*0) orientations (red line), and the Cu(*hhl*) orientations (blue line). The four quadrants with chiral orientations are marked with their chirality, *R* or *S*.

separated by monoatomic step edges with straight sections separated by monoatomic kinks. The structures are differentiated by which of the three low Miller index planes, (111), (110), or (100), form the terrace, step, or kink microfacets, respectively. The width of the terrace and the length of the straight section of the step edge further differentiate these motifs. In principle, this provides a simple conceptual framework for understanding the structure sensitivity of surface chemistry; however, experimental reality requires the preparation and study of numerous surface orientations to sample the continuous space of surface orientations adequately.

To circumvent the daunting problem of making many single-crystal surfaces and studying enantiospecific reaction kinetics on each, we have adopted an approach that requires only one sample, a surface structure spread single crystal (S^{4}C) that exposes a 2D continuum of surface orientations.[15] Figure 1b shows a photograph of a Cu(110) ± 14°-S^{4}C. The shape is spherical with the Cu(110) plane at the center and exposes all surface orientations having normal vectors within 14° of the ⟨110⟩ direction. The points along the solid blue line expose achiral surfaces with the (110) terraces separated by straight, close-packed (111) step edges. The points along the dashed red line expose achiral surfaces with the (110) terraces separated by (100) steps. The terrace widths decrease continuously from the (110) center to the sample edge where they reach ~5 Å. The quadrants between the red and blue lines expose chiral surfaces with terrace-step-kink structures. Coupled with the use of spatially resolved surface analysis methods, S^{4}C samples allow mapping of surface properties and surface reaction kinetics across a continuous distribution of surface orientations. There is a long history of using spherical and cylindrical single crystals to map qualitative trends in chemical reactivity and various physical properties across surface structure space.[16,17] Herein, we advance the methodology to allow quantitative mapping of reaction rate constants with the fidelity needed to quantify the enantiospecific reaction kinetics of chiral adsorbates; in this case, tartaric acid (TA, $HO_2CCH(OH)CH(OH)CO_2H$) decomposition on Cu(*hkl*)$^{R\&S}$ surfaces.

Tartaric acid and its salts are arguably the most famous of chiral compounds, having served as the subject of Pasteur's famous experiment linking optical activity to molecular structure.[18] TA continues to be interesting because its chemistry on single-crystal Cu surfaces is well documented.[19−25] Adsorption of a saturated monolayer of TA onto the Cu(110) at 400 K results in the formation of the deprotonated monotartrate species ($^-O_2CCH(OH)CH(OH)CO_2H$). During heating, TA decomposes to yield CO_2, H_2, CO, and some minor products including O and C atoms on the surface. One of the interesting features is that this decomposition reaction exhibits the kinetics of a vacancy-mediated explosion mechanism. For TA to decompose, adjacent empty sites onto which decomposition fragments can adsorb before desorbing into the gas phase are required. Initially, when TA saturates the surface and its coverage is high, $\theta_{TA} \cong 1$, the vacancy coverage is very low, $(1 - \theta_{TA}) \cong 0$. As a result, the explosion reaction cannot occur, until vacancies are created by an initiation process.[22] Once a sufficient coverage of vacancies has formed, the reaction follows explosive, autocatalytic kinetics in the sense that the reaction between one TA molecule and a vacancy results in the formation of two vacancies, which then react with two TAs to yield four vacancies, and so on. Thus, the rate accelerates autocatalytically, even under isothermal conditions.[22] Careful measurements of the kinetics reveal that the rate of TA decomposition on Cu surfaces is well-described by the rate law

$$r = \frac{-d\theta_{TA}}{dt} = k_i\theta_{TA} + k_e\theta_{TA}(1 - \theta_{TA})^2 \tag{1}$$

suggesting that TA decomposition actually requires the presence of two adjacent vacancies.[22,26] The first term describes an initiation process occurring at the saturation coverage and resulting in vacancy formation. Once the vacancy coverage reaches a critical value, the explosion reaction described by the second term accelerates autocatalytically. The most intriguing aspect of the explosive decomposition kinetics is that the nonlinearity of the rate law results in rates of D- and L-TA decomposition with an extremely high enantiospecificity on chiral Cu(*hkl*)$^{R\&S}$ surfaces.[12] On the Cu(643)$^{R\&S}$ surfaces, the enantiospecific rates differ by ~50×.

■ EXPERIMENTAL SECTION

S^{4}C Preparation. The Cu(110) ± 14°-S^{4}C was prepared from a commercially supplied Cu(110) single crystal (Monocrystals Inc.) ~10 mm in diameter and 2 mm in thickness. The crystal was sent to a commercial provider of nanomachining services (Empire Precision Plastics, Rochester, NY), where it was lathed using single-point diamond turning into a spherical dome with a 21 mm radius of curvature (Figure 1b). Once returned, the Cu(110) ± 14°-S^{4}C was mounted by vacuum braising (Ag−Cu eutectic braise, 72% Ag) to a 14 × 14 × 3 mm^3 Cu block. The sample was then subjected to several cycles of Ar$^+$ ion sputtering and annealing at 850 K to yield an ordered surface. Finally, the rotational orientation of the Cu lattice vectors was determined using electron backscatter diffraction (sect. SI 2).

TA/S^{4}C Surface Preparation. The experiments were conducted in a ThermoFisher ThetaProbe with a preparation chamber for sample cleaning and TA deposition and an analysis chamber for periodic sample annealing at 433 K interspersed with spatially resolved surface analysis using X-ray photoemission spectroscopy (XPS). In the analysis chamber, the S^{4}C surface was cleaned using Ar$^+$ ion sputtering followed by annealing at 900 K for 5 min. To prepare the monolayer of D-TA, the surface was heated to 400 K and then exposed to a flux of D-TA until the surface was saturated. The D-TA source was an aluminum sublimation cell heated to 390 K. The surface temperature of 400 K ensures that no TA multilayer was formed during adsorption. Under these conditions, the D-TA

DOI: 10.1021/acs.langmuir.9b02476
Langmuir 2019, 35, 16438−16443

monolayer formed on the Cu(110) region of the S^{4}C has an absolute coverage of 0.278 ML in an ordered overlayer lattice denoted by $(4,1;\bar{2},4)$.[19,21,23] For the purposes of our analysis, we normalized the fractional saturation coverage at the start of the experiment to $\theta_{\text{D-TA}}^{(hkl)}(0) = 1$.

XPS Analysis. The spatiotemporal evolution of the D-TA coverage, $\theta_{\text{D-TA}}^{(hkl)}(t)$, was measured using XPS after sequential periods of heating the surface at T_{iso} = 433 K. The heating schedule is indicated by the marks at the top of Figure 2 (sect. SI 3). There were 29 heating periods totaling 3480 s. In each case, the S^{4}C was heated at 1 K/s from ~300 to 433 K, held at 433 K for time intervals in the range of 45−600 s and then quenched at ~−1 K/s to <390 K before starting the XPS mapping of the local D-TA coverage. The annealing times were shortest over the period 1100−2000 s during which the explosive decomposition occurred most rapidly.

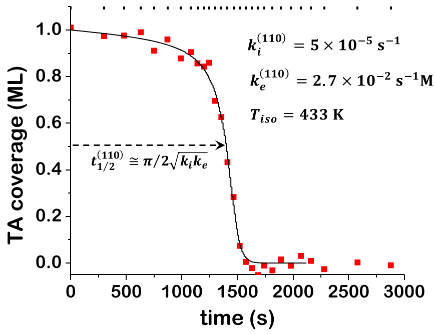

Figure 2. D-TA coverage versus time (red squares) measured at the Cu(110) point (center) on the Cu(110) ± 14°-S^{4}C. The solid black curve is a fit of the decay curve predicted by the rate law (eq 1) and parameterized by the rate constants, $k_{\text{i}}^{(110)}$ and $k_{\text{e}}^{(110)}$. The hash marks at the top indicate the distribution of the time intervals used to measure the $\theta_{\text{D-TA}}^{(hkl)}(t)$ decay curves at 169 points across the Cu(110) ± 14°-S^{4}C.

Spatially resolved XPS mapping was conducted using an X-ray spot diameter of 400 μm resulting in a ~1° spread of surface orientations over the analysis region. Mapping of the XPS signal across the S^{4}C used a grid of 169 points with a physical spacing of ~0.75 mm (sect. SI 4). Each O 1s XPS spectrum required a collection time of 5 s. The decomposition of D-TA leaves ~10% of the oxygen atoms on the surface at an extent of reaction of EOR = 100%. Consequently, the time-dependent coverage of D-TA at any given point on the surface, $\theta_{\text{D-TA}}^{(hkl)}(t)$, was estimated based on the intensity of the O 1s signal from the monolayer at that point initially, $I_{\text{O}}^{(hkl)}(0)$, and the intensity of the O 1s signal at that point after reaction completion, $I_{\text{O}}^{(hkl)}(\infty)$.

$$\theta_{\text{D-TA}}^{(hkl)}(t) = \frac{I_{\text{O}}^{(hkl)}(t) - I_{\text{O}}^{(hkl)}(\infty)}{I_{\text{O}}^{(hkl)}(0) - I_{\text{O}}^{(hkl)}(\infty)} \qquad (2)$$

■ RESULTS

The structure-sensitive, surface decomposition kinetics of D-TA were monitored at T_{iso} = 433 K as a function of time using spatially resolved X-ray photoemission spectroscopy (XPS) to measure the local D-TA coverage decay curves, $\theta_{\text{D-TA}}^{(hkl)}(t)$, at 169 points distributed across the Cu(110) ± 14°-S^{4}C (sect. SI 4). The data for $\theta_{\text{D-TA}}^{(110)}(t)$ are shown in Figure 2. The marks at the top of Figure 2 indicate the times at which the sample temperature was quenched from T_{iso} = 433 K and XPS was used to map the coverage, $\theta_{\text{D-TA}}^{(hkl)}(t)$, remaining across the S^{4}C. The spacing of sampling times is purposefully nonuniform to provide sufficient resolution over the period in which the explosion kinetics result in the most rapid coverage decay. The data in Figure 2 reveal the slow initiation process, t = 0 → 1000 s, followed by the onset and rapid completion of the explosive decomposition process, t = 1000 → 1500 s. The $\theta_{\text{D-TA}}^{(hkl)}(t)$ curves obtained from the other 168 surface orientations sampled are all qualitatively similar to $\theta_{\text{D-TA}}^{(110)}(t)$ but with $t_{1/2}^{(hkl)}$ values spanning the range 800 → 2000 s. The black curve in Figure 2 is the optimal fit of the rate law (eq 1) to the $\theta_{\text{D-TA}}^{(110)}(t)$ data, yielding estimates of $k_{\text{i}}^{(110)} = 5.0 \times 10^{-5}$ s^{-1} and $k_{\text{i}}^{(110)} = 2.7 \times 10^{-2}$ s^{-1} ML$_{\text{v}}^{-2}$, where ML$_{\text{v}}$ is the unit of vacancy coverage in monolayers. For all surface orientations, $k_{\text{e}}^{(hkl)} \gg k_{\text{i}}^{(hkl)}$. The rate law given in eq 1 has an analytical solution (sect. SI 5) that can be used to relate various features of the $\theta_{\text{D-TA}}^{(hkl)}(t)$ decay curves to $k_{\text{i}}^{(hkl)}$ and $k_{\text{e}}^{(hkl)}$. Fitting the data to either the analytical solution to eq 1 or to the numerically integrated solution yields the same results. The time to reach a coverage of $\theta_{\text{D-TA}}^{(hkl)}(t) = 0.5$ is given by $t_{1/2} \cong \pi/2\sqrt{k_{\text{i}}k_{\text{e}}}$ under the condition $k_{\text{e}} \gg k_{\text{i}}$. This relationship is particularly important because fitting the data with the rate law of eq 1 yields an accurate estimate of $k_{\text{i}}k_{\text{e}}$ (sect. SI 6), which, in turn, serves as a good measure of the enantiospecificity of TA decomposition on the chiral surface orientations.

The spatiotemporal evolution of the $\theta_{\text{D-TA}}^{(hkl)}(t)$ decay curves is illustrated in Figure 3 at 10 of the 29 time intervals used for data collection (see sect. SI 7 for the remainder). The coverage maps are ordered by the total extent of the reaction (EOR) determined by averaging the local coverage of D-TA remaining at each point across the surface, EOR = 1 − $\langle\theta_{\text{D-TA}}^{(hkl)}\rangle$. The rotational orientations of the maps with respect to the

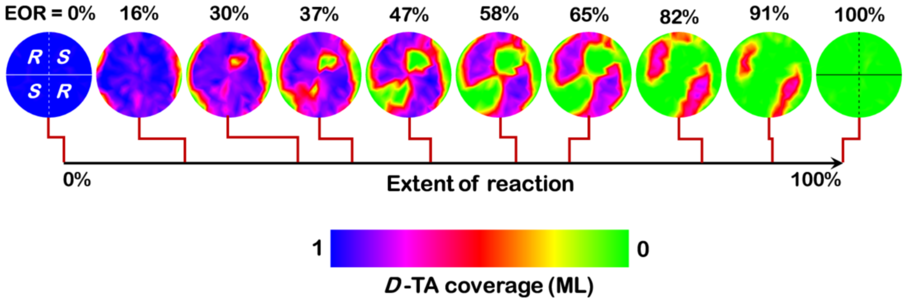

Figure 3. Maps of D-TA coverage decay, $\theta_{\text{D-TA}}^{(hkl)}(t)$, during isothermal decomposition on a Cu(110) ± 14°-S^{4}C at T_{iso} = 433 K. Maps were obtained using the O 1s XPS signal measured at 169 points distributed across the inner ±12.4° of the Cu(110) ± 14°-S^{4}C. The extent of reaction (EOR) has been estimated using the average value of $\theta_{\text{D-TA}}^{(hkl)}(t)$. The evolution of $\theta_{\text{D-TA}}^{(hkl)}(t)$ clearly reveals the 2-fold rotational symmetry of the surface structure about the central Cu(110) point. The maps shown represent 10 of 29 in the complete data set. The remainder can be found in the Supporting Information sect. SI 7.

DOI: 10.1021/acs.langmuir.9b02476
Langmuir 2019, 35, 16438−16443

crystallographic directions of the S^{4}C (Figure 1b) are marked on the EOR = 0% map. The maps at EOR = 16 and 30% show that D-TA decomposition starts at the edges of the crystal and, in particular, at the edges exposing the (111) steps. Clearly, the (111) step edges are more reactive than the (100) step edges. This initial pattern of reactivity is roughly symmetric with respect to reflection through the vertical mirror plane and is not revealing of any enantiospecificity. The maps at EOR = 47–91% reveal regions close to the center of the S^{4}C in which there is high activity in the *S*-quadrants and relatively low activity in the *R*-quadrants. This pattern is inversion symmetric but lacks symmetry with respect to reflection through the vertical and horizontal mirror planes, clearly revealing enantiospecificity. It is important to note that several related experiments have independently demonstrated the diastereomeric relationship between the decomposition kinetics of D- and L-TA on Cu$(hkl)^{R\&S}$ surfaces (sect. SI 8), $D/R \equiv L/S \not\equiv L/R \equiv D/S$.[12,13]

■ DISCUSSION

The measured $\theta_{\text{D-TA}}^{(hkl)}(t)$ decay curves at EOR = 0–100% yield estimates of the surface orientation dependence of the rate constants, $k_{\text{i}}^{(hkl)}$ and $k_{\text{e}}^{(hkl)}$, defined in eq 1. One can thereby gain insight into the fundamental origins of enantioselectivity in the D-TA decomposition process and, more importantly, the origins of its dependence on surface structure. One of the key challenges for the study of enantioselectivity is that the differences in the underlying energetics giving rise to enantiospecificity are quite small, typically on the order of a few kJ/mol. For example, as measured on a set of seven chiral Cu$(hkl)^{R\&S}$ surfaces, the enantiospecific differences in the desorption energies of *R*-3-methylcyclohexanone all lie in the range $\Delta\Delta E_{\text{des}}$ = 0.6–1.0 kJ/mol.[14] In the case of D- and L-aspartic acid ($HO_2CCH(NH_2)CH_2CO_2H$), which are structurally related to TA, the enantiospecific difference in equilibrium adsorption energies on the Cu$(3,1,17)^{R\&S}$ surfaces is $\Delta\Delta E_{\text{ads}}$ = 3.2 kJ/mol.[13] These small differences in enantiospecific energetics and the consequent need for accurate measurement are challenges to both measurement and optimization of enantioselective chiral surfaces.

In addition to allowing direct access to a continuous distribution of surface orientations on one sample, one of the important features of S^{4}C samples is that they ensure that all points on the surface are treated identically. Each surface orientation is subject to the same initial exposure to TA, temperature history, analysis conditions, etc. Thus, random errors in the differences between rate constants measured on different surface orientations are minimized. As a consequence, our data set, $\{\theta_{\text{D-TA}}^{(hkl)}(t)\}$, provides an unprecedented high resolution and high fidelity perspective on surface structure sensitive enantiospecificity.

The rate constants, $k_{\text{i}}^{(hkl)}$ and $k_{\text{e}}^{(hkl)}$, describing the D-TA decomposition on Cu$(hkl)^{R\&S}$ surfaces vicinal to Cu(110) have been estimated by fitting eq 1 to the $\theta_{\text{D-TA}}^{(hkl)}(t)$ data at each surface orientation. Figure 4a shows a map of the initiation rate constants, $k_{\text{i}}^{(hkl)}$, across the Cu(110) ± 14°-S^{4}C. The values of $k_{\text{i}}^{(hkl)}$ are roughly symmetric with respect to reflection through the vertical mirror plane, and they are greatest in the directions that expose the (111) steps edges, consistent with the observed onset of D-TA decomposition in these regions of surface orientation. In the central region of the S^{4}C, the values of $k_{\text{i}}^{(hkl)}$ are fairly insensitive to surface orientation. In short, the structure dependence of the values of $k_{\text{i}}^{(hkl)}$ does not reflect the enantiospecificity observed in the maps of $\theta_{\text{D-TA}}^{(hkl)}(t)$ shown in Figure 3.

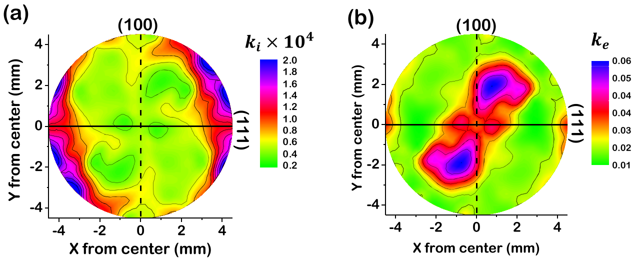

Figure 4. Maps of (a) $k_{\text{i}}^{(hkl)}$ and (b) $k_{\text{e}}^{(hkl)}$ measured at T_{iso} = 433 K across the Cu(110) ± 14°-S^{4}C. These have been rotationally averaged to conform to the 2-fold rotational symmetry of the Cu(110) surface. The ranges of value are <10× for both rate constants and at all orientations $k_{\text{e}}^{(hkl)} \gg k_{\text{i}}^{(hkl)}$. The values of k_{i} are fairly symmetric with respect to the mirror symmetry directions, while the values of k_{e} reveal the underlying chirality of the Cu(110) ± 14°-S^{4}C.

The values of the explosion rate constants, $k_{\text{e}}^{(hkl)}$, extracted from the $\theta_{\text{D-TA}}^{(hkl)}(t)$ data are shown in Figure 4b. They span a range of only a factor of ~6× and, in contrast to the values of $k_{\text{i}}^{(hkl)}$, the values of $k_{\text{e}}^{(hkl)}$ are lowest in the regions of high step density and greatest in the central region of the S^{4}C where the terraces are the widest. More importantly, the values of $k_{\text{e}}^{(hkl)}$ reveal enantiospecificity in the form of maxima that are clearly located in the *S*-oriented quadrants of the S^{4}C. The $k_{\text{e}}^{(hkl)}$ map reveals an asymmetry with respect to the horizontal and vertical mirror planes. These observations, in conjunction with the weak variation of $k_{\text{i}}^{(hkl)}$ across the central region of the S^{4}C, indicate that $k_{\text{e}}^{(hkl)}$ is primarily responsible for the observed enantiospecificity of the D-TA decomposition kinetics. The ability to resolve the roles of individual rate constants in dictating the enantioselectivity of a surface reaction is unprecedented.

In addition to allowing the estimation of enantiospecific rate constants, the $\{\theta_{\text{D-TA}}^{(hkl)}(t)\}$ data set allows identification of the surface orientation exhibiting the maximum enantiospecificity for D-TA decomposition. The practical metric often used to optimize an enantioselective process is enantiomeric excess in the product mixture, defined as ee = $|[D] - [L]|/([D] + [L])$, where $[D]$ is the concentration of the *D*-enantiomer in the product stream of the process. However, ee depends on both fundamental kinetic parameters and process parameters. Herein, we use the definitions of enantiospecificity that are based solely on fundamental kinetic quantities. Figure 5 plots the values of $t_{1/2}^{(hkl)}$, varying from 800 to 2000 s across the Cu(110) ± 14°-S^{4}C. As expected, the minima in $t_{1/2}^{(hkl)}$ lie in the

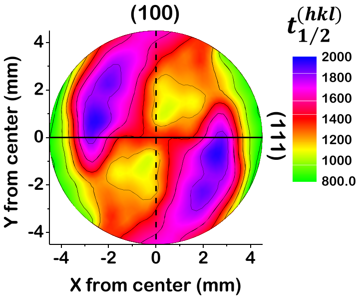

Figure 5. Map of $t_{1/2}^{(hkl)}$ across the Cu(110) ± 14°-S^{4}C. This clearly reveals the higher reactivity (lower $t_{1/2}^{(hkl)}$) of the *S*-surfaces for the decomposition of D-TA.

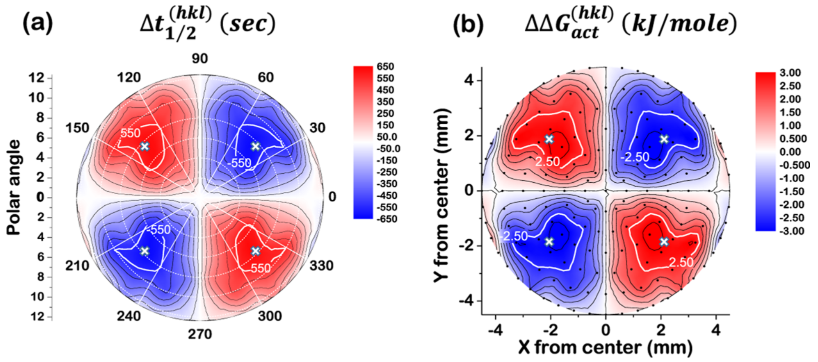

Figure 6. Maps of (a) $\Delta t_{1/2}^{(hkl)} = t_{1/2}^{(hkl)\text{-}R} - t_{1/2}^{(hkl)\text{-}S}$ and (b) $\Delta\Delta G_{\text{act}}^{(hkl)} = 2RT_{\text{iso}}\cdot\ln(k_i^S k_e^S/k_i^R k_e^R)$ across the Cu(110) ± 14°-S^{4}C. The crosses reveal the surface orientations, Cu(14,17,2)$^{R\&S}$, with greatest enantiospecificity among orientations vicinal to the Cu(110) surface.

S-quadrants of the S^{4}C where the decomposition of D-TA has the highest activity and the maxima lie in the *R*-quadrants where the D-TA remains the longest (Figure 3). Note that the values of $t_{1/2}^{(hkl)}$ are asymmetric with respect to reflection through the vertical and horizontal mirror planes of the crystal.

We define two measures of the intrinsic enantiospecificities of TA decomposition on the Cu$(hkl)^{R\&S}$ surfaces vicinal to Cu(110). The first is an observable, $\Delta t_{1/2}^{(hkl)} = t_{1/2}^{(hkl)\text{-}R} - t_{1/2}^{(hkl)\text{-}S}$ (Figure 6a), determined by subtracting the values of $t_{1/2}^{(hkl)}$ measured at points related by reflection through the vertical mirror plane (sect. SI 9). The values of $\Delta t_{1/2}^{(hkl)}$ span the range ±650 s and $\Delta t_{1/2}^{(hkl)} = 0$ along the high symmetry, achiral directions of the S^{4}C, as it must. Most importantly, the surface orientations that exhibit the maximal enantiospecificity with respect to D-TA decomposition are readily identified in the four chiral quadrants of the S^{4}C. These maxima are located in the regions with $|\Delta t_{1/2}^{(hkl)}| > 550$ s, outlined by the white contour lines. This reveals that the surface orientations with maximum enantiospecificity lie at polar angles of $\theta \approx 8°$ from the ⟨110⟩ direction and azimuthal angles of $\varphi \approx 45°$ from the high-symmetry direction exposing the (111) steps.

The second metric for the intrinsic enantiospecificity is derived from the free energies of activation for D-TA decomposition

$$\begin{aligned}\Delta\Delta G_{\text{act}}^{(hkl)} &= (\Delta G_i^R + \Delta G_e^R) - (\Delta G_i^S + \Delta G_e^S) \\ &= 2RT_{\text{iso}}\Delta\ \ln(k_i^S k_e^S/k_i^R k_e^R)\end{aligned} \tag{3}$$

The values of $\Delta\Delta G_{\text{act}}^{(hkl)}$ are mapped across the S^{4}C in Figure 6b. They span the range ±3 kJ/mol and $\Delta\Delta G_{\text{act}}^{(hkl)} = 0$ kJ/mol along the achiral high-symmetry directions, as it must. Consistent with other measurements of enantiospecific surface reaction energetics,[12−14] these are relatively small, $\Delta\Delta G_{\text{act}}^{(hkl)} \lesssim k_BT$. The fact that we can observe their surface orientation dependence is a tribute to the S^{4}Cs as samples for highly accurate measurement. The regions containing surface orientations of maximum enantiospecificity, $|\Delta\Delta G_{\text{act}}^{(hkl)}| > 2.5$ kJ/mol, are outlined in Figure 6b by the white contour line. Not too surprisingly, these orientations of high enantiospecificity span a similar region to those identified using $\Delta t_{1/2}^{(hkl)}$. Although the definition of the free energy of activation, $\Delta G_{\text{act}}^R = \Delta G_i^R + \Delta G_e^R$, depends on both the initiation and the explosion rate constants, the fact that the initiation rate constants are only weakly enantiospecific (Figure 4a) suggests that the enantiospecificity of the explosion step dominates the net enantiospecificity, $\Delta\Delta G_{\text{act}}^{(hkl)} \cong \Delta G_e^R - \Delta G_e^S$.

High enantiospecificity spans a region of surface orientation space (Figure 6) and, therefore, a distribution of closely related surface structures. The crosses in Figure 6a,b pinpoint the locations of the Cu(14,17,2)$^{R\&S}$ surfaces (Figure 1a). These are located at $(\theta, \varphi) = (7.6°, 42°)$ as defined by Figure 6a. The ideal Cu(14,17,2)^R surface structure consists of the (110) terraces that are ∼9 Å wide separated by monoatomic steps formed of the (100) and (111) microfacets (Figure 1a inset). The surfaces lying within a few degrees of Cu(14,17,2)$^{R\&S}$ have a distribution of terrace widths (decreasing at higher polar angles) and a distribution of the densities of (100) and (111) microfacets along the length of the step edge. The real surface structures are further complicated by the effects of thermal roughening due to diffusion of atoms along the step edges resulting in the coalescence of kinks. While this complicates the surface structure, it does not change the net chirality of the surface.[27−29]

■ CONCLUSIONS

The S^{4}C samples have provided unprecedented insight into the structure sensitivity of an enantiospecific surface reaction. A key aspect of this work is the ability to make measurements on multiple surfaces that have been treated identically, thereby allowing high-fidelity resolution of reaction rate constants whose values span less than an order of magnitude. The result is the ability to localize a maximum in enantioselectivity within a continuous 2D space of orientations. The most enantioselective surfaces for TA decomposition are those vicinal to Cu(14,17,2)$^{R\&S}$. More importantly, the use of the S^{4}C provides a direct insight into the mechanistic origin of this optimum; the structure dependence of $k_e^{(hkl)}$, the rate constant for the explosive decomposition of TA on surfaces vicinal to the Cu(110).

■ ASSOCIATED CONTENT

Supporting Information

The Supporting Information is available free of charge at https://pubs.acs.org/doi/10.1021/acs.langmuir.9b02476.

> Stereographic triangle of chiral surface orientations; electron backscatter diffraction of the Cu(110) ± 14°-S^{4}C; heating schedule for sampling $\theta_{\text{D-TA}}^{(hkl)}(t)$; measurement grid used for mapping of $\theta_{\text{D-TA}}^{(hkl)}(t)$; analytical solution to the D-TA/Cu decomposition rate law; residual for fitting of $\theta_{\text{D-TA}}^{(100)}(t)$ to the decomposition rate law; spatiotemporal evolution of D-TA/Cu decomposition; diastereomeric decomposition of D- and L-TA on Cu(100)-S^{4}C; definition of $\Delta t_{1/2}^{(hkl)}$ (PDF)

AUTHOR INFORMATION

Corresponding Author

*E-mail: gellman@cmu.edu. Tel: 412-268-3848.

ORCID

Aaron Reinicker: 0000-0002-5297-5884

Andrew J. Gellman: 0000-0001-6618-7427

Notes

The authors declare no competing financial interest.

ACKNOWLEDGMENTS

This work has been supported by the US NSF under grant number CHE 1764252 (final collection of data and its analysis) and by the US DOE under grant number DE SC0008703 (early envelopment of the experimental protocol).

REFERENCES

(1) Ertl, G. Reactions at surfaces: From atoms to complexity (Nobel lecture). *Angew. Chem., Int. Ed.* **2008**, *47*, 3524−3535.

(2) Spencer, N. D.; Schoonmaker, R. C.; Somorjai, G. A. Structure sensitivity in the iron single-crystal catalyzed synthesis of ammonia. *Nature* **1981**, *294*, 643−644.

(3) Nguyen, L. A.; He, H.; Pham-Huy, C. Chiral drugs: an overview. *Int. J. Biomed. Sci.* **2006**, *2*, 85−100.

(4) Lang, J. C.; Armstrong, D. W. Chiral surfaces: The many faces of chiral recognition. *Curr. Opin. Colloid Interface Sci.* **2017**, *32*, 94−107.

(5) Zaera, F. Chiral Modification of Solid Surfaces: A Molecular View. *J. Phys. Chem. C* **2008**, *112*, 16196−16203.

(6) Gellman, A. J. Chiral Surfaces: Accomplishments and Challenges. *ACS Nano* **2010**, *4*, 5−10.

(7) Hazen, R. M.; Sholl, D. S. Chiral selection on inorganic crystalline surfaces. *Nat. Mater.* **2003**, *2*, 367−374.

(8) Switzer, J. A.; Kothari, H. M.; Poizot, P.; Nakanishi, S.; Bohannan, E. W. Enantiospecific electrodeposition of a chiral catalyst. *Nature* **2003**, *425*, 490−493.

(9) McFadden, C. F.; Cremer, P. S.; Gellman, A. J. Adsorption of chiral alcohols on "chiral" metal surfaces. *Langmuir* **1996**, *12*, 2483−2487.

(10) Kelso, M. V.; Tubbesing, J. Z.; Chen, Q. Z.; Switzer, J. A. Epitaxial Electrodeposition of Chiral Metal Surfaces on Silicon(643). *J. Am. Chem. Soc.* **2018**, *140*, 15812−15819.

(11) Horvath, J. D.; Koritnik, A.; Kamakoti, P.; Sholl, D. S.; Gellman, A. J. Enantioselective separation on a naturally chiral surface. *J. Am. Chem. Soc.* **2004**, *126*, 14988−14994.

(12) Gellman, A. J.; Huang, Y.; Feng, X.; Pushkarev, V. V.; Holsclaw, B.; Mhatre, B. S. Superenantioselective Chiral Surface Explosions. *J. Am. Chem. Soc.* **2013**, *135*, 19208−19214.

(13) Yun, Y. J.; Gellman, A. J. Enantioselective Separation on Naturally Chiral Metal Surfaces: d,l-Aspartic Acid on Cu(3,1,17)$^{R\&S}$ Surfaces. *Angew. Chem., Int. Ed.* **2013**, *52*, 3394−3397.

(14) Gellman, A. J.; Huang, Y.; Koritnik, A. J.; Horvath, J. D. Structure-sensitive enantiospecific adsorption on naturally chiral Cu(hkl)$^{R\&S}$ surfaces. *J. Phys.: Condens. Matter* **2017**, *29*, No. 034001.

(15) de Alwis, A.; Holsclaw, B.; Pushkarev, V. V.; Reinicker, A.; Lawton, T. J.; Blecher, M. E.; Sykes, E. C. H.; Gellman, A. J. Surface Structure Spread Single Crystals (S^{4}Cs): Preparation and characterization. *Surf. Sci.* **2013**, *608*, 80−87.

(16) Linder, E. G. Photo-electric effect and surface structure in zinc single crystals. *Phys. Rev.* **1927**, *30*, 649−655.

(17) Gwathmey, A. T.; Benton, A. F. Some experiments showing the directional reactivities of single crystals of copper. *Trans. Electrochem. Soc.* **1939**, *77*, 211−222.

(18) Pasteur, J. L. Sur les relations qui peuvent exister enter la forme cristalline, la composition chimique et le sens de la polarisation rotatoire. *Ann. Chim. Phys.* **1848**, *24*, 442−459.

(19) Lorenzo, M. O.; Baddeley, C. J.; Muryn, C.; Raval, R. Extended surface chirality from supramolecular assemblies of adsorbed chiral molecules. *Nature* **2000**, *404*, 376−379.

(20) Lorenzo, M. O.; Humblot, V.; Murray, P.; Baddeley, C. J.; Haq, S.; Raval, R. Chemical transformations, molecular transport, and kinetic barriers in creating the chiral phase of (R,R)-tartaric acid on Cu(110). *J. Catal.* **2002**, *205*, 123−134.

(21) Behzadi, B.; Romer, S.; Fasel, R.; Ernst, K. H. Chiral recognition in surface explosion. *J. Am. Chem. Soc.* **2004**, *126*, 9176−9177.

(22) Mhatre, B. S.; Pushkarev, V.; Holsclaw, B.; Lawton, T. J.; Sykes, E. C. H.; Gellman, A. J. A Window on Surface Explosions: Tartaric Acid on Cu(110). *J. Phys. Chem. C* **2013**, *117*, 7577−7588.

(23) Romer, S.; Behzadi, B.; Fasel, R.; Ernst, K. H. Homochiral conglomerates and racemic crystals in two dimensions: Tartaric acid on Cu(110). *Chem. - Eur. J.* **2005**, *11*, 4149−4154.

(24) Rieger, A.; Sax, C.; Bauert, T.; Wackerlin, C.; Ernst, K. H. Chiral molecules adsorbed on a solid surface: Tartaric acid diastereomers and their surface explosion on Cu(111). *Chirality* **2018**, *30*, 369−377.

(25) Parschau, M.; Behzadi, B.; Romer, S.; Ernst, K. H. Stereoisomeric influence on 2D lattice structure: achiral meso-tartaric acid versus chiral tartaric acid. *Surf. Interface Anal.* **2006**, *38*, 1607−1610.

(26) Kondratyuk, P.; Karagoz, B.; Yun, Y. J.; Gellman, A. J. Initiation of Vacancy-Mediated, Surface Explosion Reactions: Tartaric and Aspartic Acid on Cu Surfaces. *J. Phys. Chem. C* **2019**, *123*, 18978−18985.

(27) Giesen, M.; Linke, U.; Ibach, H. Restructuring of the vicinal Cu(997) surface. *Surf. Sci.* **1997**, *389*, 264−271.

(28) Power, T. D.; Asthagiri, A.; Sholl, D. S. Atomically detailed models of the effect of thermal roughening on the enantiospecificity of naturally chiral platinum surfaces. *Langmuir* **2002**, *18*, 3737−3748.

(29) Baber, A. E.; Gellman, A. J.; Sholl, D. S.; Sykes, E. C. H. The real structure of naturally chiral Cu{643}. *J. Phys. Chem. C* **2008**, *112*, 11086−11089.

DOI: 10.1021/acs.langmuir.9b02476
Langmuir 2019, 35, 16438−16443